

SiMaN: Sign-to-Magnitude Network Binarization

Mingbao Lin¹ Rongrong Ji^{1,2} Zihan Xu¹ Baochang Zhang³ Fei Chao¹ Mingliang Xu⁴ Chia-Wen Lin⁵
Ling Shao⁶

Abstract

Binary neural networks (BNNs) have attracted broad research interest due to their efficient storage and computational ability. Nevertheless, a significant challenge of BNNs lies in handling discrete constraints while ensuring bit entropy maximization, which typically makes their weight optimization very difficult. Existing methods relax the learning using the sign function, which simply encodes positive weights into +1s, and -1s otherwise. Alternatively, we formulate an angle alignment objective to constrain the weight binarization to $\{0, +1\}$ to solve the challenge. In this paper, we show that our weight binarization provides an analytical solution by encoding high-magnitude weights into +1s, and 0s otherwise. Therefore, a high-quality discrete solution is established in a computationally efficient manner without the sign function. We prove that the learned weights of binarized networks roughly follow a Laplacian distribution that does not allow entropy maximization, and further demonstrate that it can be effectively solved by simply removing the ℓ_2 regularization during network training. Our method, dubbed sign-to-magnitude network binarization (SiMaN), is evaluated on CIFAR-10 and ImageNet, demonstrating its superiority over the sign-based state-of-the-arts. Code is at <https://github.com/lmbxmu/SiMaN>.

1. Introduction

Deep neural networks (DNNs), especially convolutional neural networks (CNNs), have been effectively used in many tasks of computer vision, such as image recognition (He et al., 2016), object detection (Redmon et al., 2016), and semantic segmentation (Long et al., 2015). Nowadays, DNNs

are almost trained on high-capacity but power-hungry graphics processing units (GPUs); however, such DNN models often fail to run on low-power devices. As a result, substantial efforts have been invested in accelerating DNNs. Typical methods include, but are not limited to, network pruning (Lin et al., 2020c; Evci et al., 2020; Lin et al., 2020a), tensor decomposition (Jaderberg et al., 2014; Kim et al., 2019; Hayashi et al., 2019) and low-precision quantization (Cai et al., 2017; Yang et al., 2019; Han et al., 2020).

In particular, binary neural networks (BNNs), which quantize their weights and activations in a 1-bit binary form, have attracted increasing attention for two major reasons: 1) The memory usage of a BNN is $32\times$ lower than its full-precision counterpart, since the weights of the latter are stored in a 32-bit floating-point form. 2) A significant reduction of computational complexity can be achieved by executing efficient XNOR and bitcount operations, *e.g.*, up to $58\times$ speed-ups on CPUs as reported by (Rastegari et al., 2016). Nevertheless, BNNs are also famed for their significant performance degradation. For example, XNOR-Net (Rastegari et al., 2016) suffers an 18% drop in top-1 accuracy when binarizing ResNet-18 on the ImageNet classification task (Deng et al., 2009). This greatly restricts the deployment of BNNs.

One major obstacle in BNN is the discrete constraints imposed on the pursued binary weights, which challenge the weight optimization. Meanwhile, BNNs also require the two possible values of binarized weights to be uniformly (half-half) distributed to ensure bit entropy maximization. To this end, most existing approaches simply employ the sign function to binarize weights where positive weights are encoded into +1s, and -1s are used otherwise (Rastegari et al., 2016; Lin et al., 2017; Liu et al., 2018; Qin et al., 2020b; Lin et al., 2020b). To compensate for the entropy information, recent methods, such as Bayesian optimization (Gu et al., 2019b), rotation matrix (Lin et al., 2020b), and weight standardization (Qin et al., 2020b), learn a two-mode distribution for real-valued weights to increase the probability of encoding one half of the weights into +1s and the other half into -1s by the sign function. These strategies, however, increase the learning complexity, since the optimization involves additional training loss terms and variables. Moreover, it is unclear whether the simple usage of the sign function is the optimal encoding option.

¹MAC Lab, Department of Artificial Intelligence, School of Informatics, Xiamen University ²Institute of Artificial Intelligence, Xiamen University ³Beihang University ⁴Zhengzhou University ⁵National Tsing Hua University ⁶Inception Institute of Artificial Intelligence. Correspondence to: Rongrong Ji <rrji@xmu.edu.cn>.

In this paper, a novel sign-to-magnitude network binarization (SiMaN) is proposed to discretely encode DNNs, leading to improved accuracy. Within our method, we reformulate the recent angle alignment objective (Lin et al., 2020b), which aims to maximize the cosine distance between the full-precision weight vector and its encoded binarization. Different from existing works that binarize weights into $\{-1, +1\}$ by the sign function, our binarization falls into $\{0, +1\}$. In this way, we reveal that the globally analytical binarization for our angle alignment can be found in a computationally efficient manner of $\mathcal{O}(n \log n)$ by quantizing into +1s the high-magnitude weights, and 0s otherwise, therefore enabling weight binarization without the sign function. To the best of our knowledge, we prove for the first time that the learned real-valued weights roughly follow a Laplacian distribution, which results in around 37% of weights being encoded into +1s. This prevents the BNN from maximizing the entropy of information. To solve this, we do not add a term to the loss function since this increases the optimization difficulty. Alternatively, we analyze the intrinsic numerical values of weights, and show that the simple removal of the ℓ_2 regularization destroys the Laplacian distribution, and thus enhances the half-half weight binarization. As a result, the final binarization is obtained by encoding into +1s weights within the largest top-half magnitude, and 0s otherwise to further reduce the computational complexity from $\mathcal{O}(n \log n)$ to $\mathcal{O}(n)$.

In summary, this paper makes the following contributions:

- A new learning objective based on the angle alignment is proposed and a magnitude-based analytical solution is developed in a computationally efficient manner.
- We formally prove that the learned weights in BNNs follow a Laplacian distribution, which, as revealed, prevents the maximization of bit entropy.
- A detailed analysis on the numerical values of weights shows that simply removing the ℓ_2 regularization benefits maximizing the bit entropy while further reducing the computational complexity.
- Experiments on CIFAR-10 (Krizhevsky et al., 2009) and ImageNet (Deng et al., 2009) demonstrate that our sign-to-magnitude framework for network binarization outperforms the traditional sign-based binarization.

2. Related Work

Following the introduction of pioneering research (Courbariaux et al., 2016) where the sign function and the straight-through estimator (STE) (Bengio et al., 2013) are respectively adopted for the forward weight/activation binarization and backward gradient updating, BNNs have emerged as one of the most appealing approaches for the deployment

of DNNs in resource-limited devices. As such, great efforts have been put into closing the gap between full-precision networks and their BNNs. In what follows, we briefly review some related works. A comprehensive overview can be found in the survey papers (Simons & Lee, 2019; Qin et al., 2020a).

XNOR-Net (Rastegari et al., 2016) introduces two scaling factors for channel-wise weights and activations to minimize quantization error. Inspired by this, XNOR-Net++ (Bulat & Tzimiropoulos, 2019) improves the performance by integrating the two scaling factors into one, which is then updated using the standard gradient propagation. Except for the scaling factors, RBNN (Lin et al., 2020b) further reduces the quantization error by optimizing the angle difference between a full-precision weight vector and its binarization. To enable the gradient propagation and reduce the “gradient mismatch” by the STE (Bengio et al., 2013), several works, such as the swish function (Darabi et al., 2018), piece-wise polynomial function (Liu et al., 2018), and error decay estimator (Qin et al., 2020b), formulate the forward/backward quantization as a differentiable non-linear mapping.

Another direction circumvents the gradient approximation of the sign function by sampling from the weight distribution (Peters & Welling, 2018; Shayer et al., 2018). There are also abundant works that explore the optimization of BNNs (Leng et al., 2018; Alizadeh et al., 2018; Bethge et al., 2019; Helwegen et al., 2019; Martinez et al., 2019) and explain their effectiveness (Anderson & Berg, 2018). Recent works (Darabi et al., 2018; Gu et al., 2019a) embed various regularization terms into the training loss to binarize the weights and control the activation ranges (Ding et al., 2019). Moreover, other recent studies devise binarization-friendly structures to boost the performance. For example, Bi-Real (Liu et al., 2018) designs double residual connections with full-precision downsampling layers. XNOR-Net++ (Bulat & Tzimiropoulos, 2019) replaces ReLU by PReLU. ReActNet (Liu et al., 2020) adds parameter-free shortcuts on MobileNetV1 (Howard et al., 2017) and the group convolution is replaced by a regular convolution.

3. Binary Neural Networks

For an L -layer CNN model, we denote $\mathbf{W}^i = \{\mathbf{w}_1^i, \mathbf{w}_2^i, \dots, \mathbf{w}_{c_{out}^i}^i\} \in \mathbb{R}^{n^i \times c_{out}^i}$ as the real-valued weight set for the i -th layer, where $\mathbf{w}_j^i \in \mathbb{R}^{n^i}$ denotes the j -th weight. The real-valued input activations of the i -th layer are represented as $\mathbf{A}^i = \{\mathbf{a}_1^i, \mathbf{a}_2^i, \dots, \mathbf{a}_{c_{in}^i}^i\} \in \mathbb{R}^{m^i \times c_{in}^i}$; here, c_{out}^i and c_{in}^i respectively represent the output and input channels, and n^i and m^i denote the size of each weight and input, respectively. Then, the convolution result is expressed by

$$\mathbf{a}_j^{i+1} = \mathbf{w}_j^i \circledast \mathbf{A}^i, \quad (1)$$

where \otimes stands for the convolution operation. For simplicity, we omit the non-linear layer here.

In a BNN, the real-valued \mathbf{w}_j^i and \mathbf{A}^i in Eq. (1) are quantized into binary values $(\mathbf{b}_w)_j^i \in \{-1, +1\}^{n^i}$ and $(\mathbf{B}_A)^i \in \{-1, +1\}^{c_{in} \times m^i}$, respectively. As a result, the convolution result can be approximated as

$$\mathbf{a}_j^{i+1} \approx \beta_j^i \cdot (\mathbf{b}_w)_j^i \otimes (\mathbf{B}_A)^i, \quad (2)$$

where β_j^i is a channel-level scaling factor (Rastegari et al., 2016; Bulat & Tzimiropoulos, 2019).

For the implementation of the BNN training, the forward calculation is fulfilled by conducting the convolution between $(\mathbf{b}_w)_j^i$ and $(\mathbf{B}_A)^i$ in Eq. (2), whereas their real-valued counterparts, \mathbf{w}_j^i and \mathbf{A}^i , are updated during backpropagation. To this end, following (Hubara et al., 2016; Bulat & Tzimiropoulos, 2019; Lin et al., 2020b), the activation binarization in this work is simply realized by the sign function,

$$(\mathbf{B}_A)^i = \text{sign}(\mathbf{A}^i) = \begin{cases} +1, & \text{if } \mathbf{A}^i \geq 0, \\ -1, & \text{otherwise.} \end{cases} \quad (3)$$

In the backpropagation phase, we adopt the piece-wise polynomial function (Liu et al., 2018) to approximate the gradient of a given loss \mathcal{L} w.r.t. the input activations \mathbf{A}^i as follows

$$\frac{\partial \mathcal{L}}{\partial \mathbf{A}^i} = \frac{\partial \mathcal{L}}{\partial (\mathbf{B}_A)^i} \cdot \frac{\partial (\mathbf{B}_A)^i}{\partial (\mathbf{A}^i)} \approx \frac{\partial \mathcal{L}}{\partial (\mathbf{B}_A)^i} \cdot \frac{\partial F(\mathbf{A}^i)}{\partial \mathbf{A}^i}, \quad (4)$$

where $\frac{\partial F(\mathbf{A}^i)}{\partial \mathbf{A}^i}$ is defined by

$$\frac{\partial F(\mathbf{A}^i)}{\partial \mathbf{A}^i} = \begin{cases} 2 + 2\mathbf{A}^i, & \text{if } -1 \leq \mathbf{A}^i < 0, \\ 2 - 2\mathbf{A}^i, & \text{if } 0 \leq \mathbf{A}^i < 1, \\ 0, & \text{otherwise.} \end{cases} \quad (5)$$

Besides, the STE (Bengio et al., 2013) is used to calculate the gradient of the loss \mathcal{L} w.r.t. the weight \mathbf{w}_j^i as

$$\frac{\partial \mathcal{L}}{\partial \mathbf{w}_j^i} = \frac{\partial \mathcal{L}}{\partial (\mathbf{b}_w)_j^i} \cdot \frac{\partial (\mathbf{b}_w)_j^i}{\partial \mathbf{w}_j^i} \approx \frac{\partial \mathcal{L}}{\partial (\mathbf{b}_w)_j^i}. \quad (6)$$

Our insight. For practical deployment, the weights and activations are quantized to $\{0, 1\}$ space instead of $\{-1, +1\}$ in order to support the efficient XNOR and bitcount logics provided by the hardware, which can be realized by setting

$$(\bar{\mathbf{B}}_A)^i = (1 + (\mathbf{B}_A)^i)/2. \quad (7)$$

$$(\bar{\mathbf{b}}_w)_j^i = (1 + (\mathbf{b}_w)_j^i)/2. \quad (8)$$

Then, the approximated convolution in Eq. (2) becomes

$$\beta_j^i \cdot (\mathbf{b}_w)_j^i \otimes (\mathbf{B}_A)^i = \beta_j^i \cdot (2 \cdot (\bar{\mathbf{b}}_w)_j^i \odot (\bar{\mathbf{B}}_A)^i - n^i), \quad (9)$$

where \odot represents the XNOR and bitcount operations that are well-fitted for real-time network inference.

In this paper, we focus on binarizing the real-valued weight \mathbf{w}_j^i . Different from most existing works (Hubara et al., 2016; Zhou et al., 2016; Bulat & Tzimiropoulos, 2019; Lin et al., 2020b), which project weights \mathbf{w}_j^i into $\mathbf{b}_w \in \{-1, +1\}^{n^i}$ using the sign function, we directly seek to encode the weights into $\bar{\mathbf{b}}_w \in \{0, +1\}^{n^i}$ and then devise an efficient optimization to attain the optimal solution in Sec. 4.1. We demonstrate in Sec. 4.2 that the weight, \mathbf{w}_j^i , roughly follows a Laplacian distribution, which inhibits the entropy maximization. We reveal that this can be easily addressed by removing the ℓ_2 regularization in Sec. 4.3.

For simplicity, the scripts “ i ” and “ j ” are omitted in the following context.

4. Weight Binarization

In this section, we specify the formulation of our weight binarization, including the binary learning objective, weight distribution, and bit entropy maximization.

4.1. Learning Objective

Our learning objective for the weight binarization is mainly inspired by the recent angle alignment proposed in (Lin et al., 2020b), which is originally formulated as

$$\arg \max_{\mathbf{R}} \frac{\text{sign}(\mathbf{R}^T \mathbf{w})^T (\mathbf{R}^T \mathbf{w})}{\|\text{sign}(\mathbf{R}^T \mathbf{w})\|_2 \|\mathbf{R}^T \mathbf{w}\|_2}, \quad (10)$$

s.t. $\mathbf{R}^T \mathbf{R} = \mathbf{I}_n,$

where \mathbf{R} is constrained to an n -order rotation matrix. As shown in Fig. 1(a), by applying the sign function on the rotated weight vector $\mathbf{R}^T \mathbf{w}$, we attain the binarization of \mathbf{w} , i.e., $\mathbf{b}_w \in \text{sign}(\mathbf{R}^T \mathbf{w})$. Thus, Eq. (10) aims to learn a rotation matrix such that the angle bias between the rotated weight vector and its encoded binarization is reduced by the sign function. However, the learning complexity of the rotation matrix, \mathbf{R} , is very high. Though a bi-rotation scenario was proposed in (Lin et al., 2020b) to learn two smaller rotation matrices, this inevitably brings more variables to optimize. Moreover, it is still unclear whether a simple application of the sign function is the optimal encoding option for the weight binarization.

To achieve high-quality weight binarization, different from the existing work (Lin et al., 2020b), we formulate our learning objective as

$$\arg \max_{\bar{\mathbf{b}}_w} \frac{(\bar{\mathbf{b}}_w)^T |\mathbf{w}|}{\|\bar{\mathbf{b}}_w\|_2 \|\mathbf{w}\|_2}, \quad (11)$$

s.t. $\bar{\mathbf{b}}_w \in \{0, +1\}^n,$

where $|\cdot|$ returns the absolute result of its input.

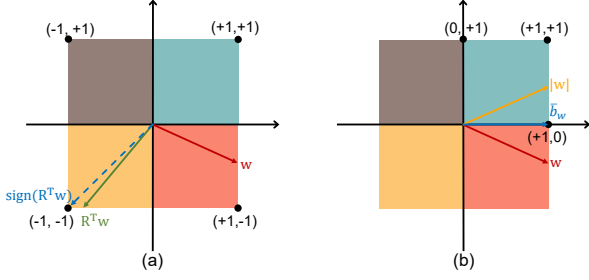


Figure 1. Comparison between (a) RBNN (Lin et al., 2020b) and (b) our SiMaN. RBNN learns a rotation matrix \mathbf{R} first, and then applies the sign function to binarize the rotated weight $\mathbf{b}_w = \text{sign}(\mathbf{R}^T \mathbf{w}) \in \{-1, +1\}^n$. In contrast, ours involves the magnitude of the weight, and then discretely learns $\bar{\mathbf{b}}_w \in \{0, 1\}^n$.

As can be seen, our learning objective is also built on the basis of angle alignment. Nevertheless, our method differs from Eq. (10) in many aspects: First, we drop the sign function since variables in a binarized network must be retained in a discrete set; thus, the binarization should be built upon the concept of the discrete optimization rather than the simple sign function. Second, we encode the weights into $\bar{\mathbf{b}}_w \in \{0, +1\}^n$ rather than $\mathbf{b}_w \in \{-1, +1\}^n$. In the following, we show that $\bar{\mathbf{b}}_w$ allows us to find an analytical solution in an efficient manner by transferring the high-magnitude weights to +1s and 0s otherwise. Third, our angle alignment is independent of the rotation matrix, \mathbf{R} , since we remove the sign function, which makes the rotation direction unpredictable. Lastly, we align the angle difference between the binarization and absolute weight vector, $|\mathbf{w}|$, instead of the weight \mathbf{w} itself. The rationale behind this is that our binarization falls into the non-negative set $\bar{\mathbf{b}}_w$. Fig. 1(b) outlines our binarization process.

Note that $\|\mathbf{w}\|_2$ is irrelevant to the optimization of Eq. (11). Thus, the learning can be simplified to

$$\begin{aligned} \arg \max_{\bar{\mathbf{b}}_w} \quad & \frac{(\bar{\mathbf{b}}_w)^T}{\|\bar{\mathbf{b}}_w\|_2} |\mathbf{w}|, \\ \text{s.t.} \quad & \bar{\mathbf{b}}_w \in \{0, +1\}^n. \end{aligned} \quad (12)$$

This is an integer programming problem (Conforti et al., 2014). Nevertheless, as demonstrated in Corollary 1, by learning the encoding space in $\{0, +1\}^n$, we can reach the global maximum in a substantially efficient fashion.

Corollary 1. For Eq. (12), the computational complexity of finding the global optimum is $\mathcal{O}(n \log n)$.

Proof: For $\bar{\mathbf{b}}_w \in \{0, +1\}^n$, it is intuitive to see that $\|\bar{\mathbf{b}}_w\|_2$ falls into the set $\{\sqrt{1}, \dots, \sqrt{n}\}$. Considering that $\|\bar{\mathbf{b}}_w\|_2 = \sqrt{k}$ ($k = 1, \dots, n$), the integer programming problem in Eq. (12) can be maximized by encoding to +1s those elements of $\bar{\mathbf{b}}_w$ that correspond to the largest k entries of $|\mathbf{w}|$. To this end, we need to perform sorting upon $|\mathbf{w}|$, for

which the complexity is $\mathcal{O}(n \log n)$. Since k has n possible values, we need to evaluate Eq. (12) n times, and then select the $\bar{\mathbf{b}}_w$ that maximizes the objective function, leading to a linear complexity with n . Hence, the overall complexity is $\mathcal{O}(n \log n)$. ■

Therefore, given one filter weight $\mathbf{w} \in \mathbb{R}^n$, we can find the binarization $\bar{\mathbf{b}}_w \in \{0, +1\}^n$ having the smallest angle with $|\mathbf{w}|$. Note that $\bar{\mathbf{b}}_w$ found in this way is the global optimum. Furthermore, we emphasize that the proof of Corollary 1 indicates that the binarization in our framework involves the magnitudes of weights instead of the signs of weights, which significantly differentiates our work from existing works. In the next two sections, we show that the overall complexity can be further reduced to $\mathcal{O}(n)$, given the bit entropy maximization.

4.2. Weight Distribution

The capacity of a binarization model, often measured by the bit entropy, is maximized when it is half-half distributed, *i.e.*, one half of the weights are encoded into 0 and the other half are encoded into +1 (Lin et al., 2020b; Qin et al., 2020b). In this case, we expect to maximize our objective in Eq. (12) when those weights with the top-half magnitudes are encoded into +1s and the remaining are encoded into 0s. However, we reveal that it is difficult to binarize \mathbf{w} with entropy maximization due to its specific form of distribution.

Specifically, after training, $w \in \mathbf{w}$ is widely believed to roughly obey a zero-mean Laplacian distribution, *i.e.*, $w \sim \text{La}(0, b)$, or a zero-mean Gaussian distribution, *i.e.*, $w \sim \mathcal{N}(0, \sigma^2)$ (Cai et al., 2017; Banner et al., 2018; Zhong et al., 2020). In Corollary 2, for the first time, we demonstrate its specific distribution.

Corollary 2. $w \in \mathbf{w}$ roughly follows a zero-mean Laplacian distribution.

Proof: Suppose w is encoded into +1 if $|w| > t$, and 0 otherwise. Note that the learning of Eq. (12) can also be regarded as a problem of finding the centroid of a subset (Shakarji & Srinivasan, 2013), which can be calculated by the integral:

$$\begin{aligned} \frac{(\bar{\mathbf{b}}_w)^T}{\|\bar{\mathbf{b}}_w\|_2} |\mathbf{w}| &= \frac{\int_{-\infty}^{-t} w f(w) dw + \int_t^{+\infty} w f(w) dw}{\sqrt{\int_{-\infty}^{-t} f(w) dw + \int_t^{+\infty} f(w) dw}} \\ &= \frac{2 \int_t^{+\infty} w f(w) dw}{\sqrt{2 \int_t^{+\infty} f(w) dw}}, \end{aligned} \quad (13)$$

where $f(w)$ denotes the probability density function. Let p_{+1} denote the proportion of \mathbf{w} being encoded into +1s, which can be calculated by

$$p_{+1} = 1 - 2 \int_0^t f(w) dw. \quad (14)$$

Here, we first derive the theoretical values of p_{+1} when $p(w)$ follows a Laplacian or Gaussian distribution, and then experimentally verify our proof.

Laplacian distribution. In this case, we have $f(w) = \frac{1}{2b}e^{-w/b}$. Therefore, Eq. (13) becomes

$$\begin{aligned} \frac{(\bar{\mathbf{b}}_w)^T}{\|\bar{\mathbf{b}}_w\|_2} |\mathbf{w}| &= \frac{2 \int_t^{+\infty} \frac{w}{2b} e^{-w/b} dw}{\sqrt{2 \int_t^{+\infty} \frac{1}{2b} e^{-w/b} dw}} \\ &= \frac{(b+t)e^{-t/b}}{\sqrt{e^{-t/b}}} \\ &= (b+t)\sqrt{e^{-t/b}}. \end{aligned} \quad (15)$$

Setting $\frac{\partial(b+t)\sqrt{e^{-t/b}}}{\partial t} = 0$ to attain the maximum of Eq. (15), we have $t = b$. The proportion of +1s can be obtained as

$$p_{+1} = 1 - 2 \int_0^t \frac{1}{2b} e^{-w/b} dw \approx 0.37. \quad (16)$$

Gaussian distribution. In this case, we have $f(w) = \frac{1}{\sqrt{2\pi}\sigma} e^{-w^2/(2\sigma^2)}$. Similarly, Eq. (13) can be rewritten as

$$\begin{aligned} \frac{(\bar{\mathbf{b}}_w)^T}{\|\bar{\mathbf{b}}_w\|_2} |\mathbf{w}| &= \frac{2 \int_t^{+\infty} \frac{w}{\sqrt{2\pi}\sigma} e^{-w^2/(2\sigma^2)} dw}{\sqrt{2 \int_t^{+\infty} \frac{1}{\sqrt{2\pi}\sigma} e^{-w^2/(2\sigma^2)} dw}} \\ &= \frac{\frac{\sigma}{\sqrt{2\pi}} e^{-t^2/(2\sigma^2)}}{\sqrt{\frac{1}{2} \operatorname{erfc}\left(\frac{t}{\sqrt{2}\sigma}\right)}}, \end{aligned} \quad (17)$$

where $\operatorname{erfc}(\cdot)$ denotes the complementary error function.¹

Let $m = \frac{t}{\sqrt{2}\sigma}$, then Eq. (17) can be written as

$$\frac{(\bar{\mathbf{b}}_w)^T}{\|\bar{\mathbf{b}}_w\|_2} |\mathbf{w}| = \frac{\sigma}{\sqrt{\pi}} \frac{e^{-m^2}}{\sqrt{\operatorname{erfc}(m)}}. \quad (18)$$

Setting $\frac{\partial e^{-m^2}/\sqrt{\operatorname{erfc}(m)}}{\partial m} = 0$, we have $m = \frac{t}{\sqrt{2}\sigma} \approx 0.43$.

Thus, we obtain $t \approx 0.43\sqrt{2}\sigma$, and then derive the proportion of +1s:

$$p_{+1} = 1 - 2 \int_0^t \frac{1}{\sqrt{2\pi}\sigma} e^{-w^2/(2\sigma^2)} dw \approx 0.54. \quad (19)$$

As mentioned above, the trained weight $w \in \mathbf{w}$ obeys either a Laplacian distribution (with $p_{+1} \approx 0.37$) or a Gaussian distribution (with $p_{+1} \approx 0.54$). In Fig. 2(a), we conduct an experiment which shows a practical p_{+1} of around 0.36 after training.² This implies that $w \in \mathbf{w}$ follows a Laplacian distribution, and our proof is completed. ■

¹https://en.wikipedia.org/wiki/Error_function.

²Similar phenomena can be observed in other layers and networks as well (see Appendix A).

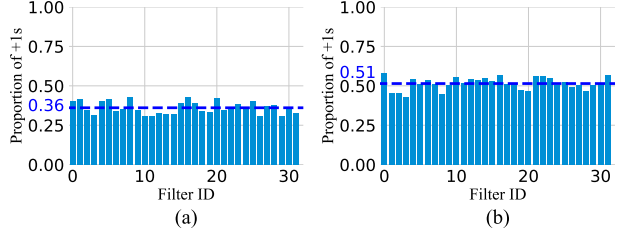


Figure 2. Proportion of +1s trained (a) with and (b) without the ℓ_2 regularization (Layer2.1.2 of ResNet-20). The dashed blue lines denote the average proportions of +1s of all filter weights.

4.3. Maximizing Bit Entropy

The proof of Corollary 1 indicates that the binarization in our framework is related to the weight magnitude, *i.e.*, $|\mathbf{w}|$. However, the Laplacian distribution contradicts the entropy maximization. To solve this, one naive solution is to assign the top half of elements of the sorted $|\mathbf{w}|$ with +1 and assign the remaining elements with 0, that is

$$\tilde{\mathbf{b}}_w = \begin{cases} +1, & \text{top half of sorted } |\mathbf{w}|, \\ 0, & \text{otherwise.} \end{cases} \quad (20)$$

Despite helping achieve entropy maximization, such a simple operation violates the learning objective of minimizing the angular bias in Eq. (12) since $\tilde{\mathbf{b}}_w$ deviates significantly from the optimal $\bar{\mathbf{b}}_w$ as revealed in Corollary 3.

Corollary 3. Suppose $\bar{\mathbf{b}}_w$ is a binarized vector with a total of k +1s and the binarized vector $\tilde{\mathbf{b}}_w$ has r different bits from $\bar{\mathbf{b}}_w$. Then the angle between $\bar{\mathbf{b}}_w$ and $\tilde{\mathbf{b}}_w$ is bounded by $[\arccos \sqrt{\frac{k}{k+r}}, \arccos \sqrt{\frac{k-r}{k}}]$.

Proof: To find the lower bound, we need to obtain $\tilde{\mathbf{b}}_w$ such that $\frac{(\bar{\mathbf{b}}_w)^T \tilde{\mathbf{b}}_w}{\|\bar{\mathbf{b}}_w\|_2 \|\tilde{\mathbf{b}}_w\|_2}$ is maximized. Intuitively, this can be achieved when $\tilde{\mathbf{b}}_w$ has all ones at the same positions as $\bar{\mathbf{b}}_w$, and r additional ones in the remaining positions, in which $\|\tilde{\mathbf{b}}_w\|_2 = \sqrt{k+r}$ and $(\bar{\mathbf{b}}_w)^T \tilde{\mathbf{b}}_w = k$. Then, we have the lower bound of $\arccos \sqrt{\frac{k}{k+r}}$. To obtain the upper bound, we need to minimize $\frac{(\bar{\mathbf{b}}_w)^T \tilde{\mathbf{b}}_w}{\|\bar{\mathbf{b}}_w\|_2 \|\tilde{\mathbf{b}}_w\|_2}$, which can be done when there are $(k-r)$ +1s in $\tilde{\mathbf{b}}_w$ in the common positions with $\bar{\mathbf{b}}_w$ and the rest are set to zeros. In this case, we have $\|\tilde{\mathbf{b}}_w\|_2 = \sqrt{k-r}$ and $(\bar{\mathbf{b}}_w)^T \tilde{\mathbf{b}}_w = k-r$, which leads to the upper bound of $\arccos \sqrt{\frac{k-r}{k}}$.

According to Corollary 2 and Eq. (20), we have $k \approx 0.37n$, and $r \approx 0.13n$. Then, we can derive the practical angle bounds as $[\arccos \sqrt{\frac{0.37}{0.37+0.13}}, \arccos \sqrt{\frac{0.37-0.13}{0.37}}] \approx [30.66^\circ, 36.35^\circ]$. Therefore, a large angle bias occurs between the solution $\tilde{\mathbf{b}}_w$ from Eq. (20) and the solution $\bar{\mathbf{b}}_w$ from optimizing Eq. (12). In Sec. 5.3, we demonstrate the poor performance when simply using $\tilde{\mathbf{b}}_w$.

Instead of imposing an additional loss term to regularize the ideal half-half binarization, we analyze the numerical value of each weight and reveal that simply removing the ℓ_2 regularization can explicitly maximize the bit capacity, leading to a more informative binarized network.

Let $\mathcal{L}_{\mathbf{b}_w}^k = \arg \max_{\mathbf{b}_w} \frac{(\mathbf{b}_w)^T}{\sqrt{k}} |\mathbf{w}| = \frac{\sum_{i=1}^k \tilde{w}_i}{\sqrt{k}}$ denote the maximum result of the integer programming problem in Eq. (12), where $\tilde{w}_i \in |\mathbf{w}|$ corresponds to the i -th largest magnitude. We have $\mathcal{L}_{\mathbf{b}_w}^{k+1} < \mathcal{L}_{\mathbf{b}_w}^k$, i.e.,

$$\frac{\tilde{w}_{k+1} + \sum_{i=1}^k \tilde{w}_i}{(\sqrt{k+1} - \sqrt{k}) + \sqrt{k}} < \frac{\sum_{i=1}^k \tilde{w}_i}{\sqrt{k}}. \quad (21)$$

We can deduce that

$$\tilde{w}_{k+1} < \mathcal{L}_{\mathbf{b}_w}^k (\sqrt{k+1} - \sqrt{k}). \quad (22)$$

For Laplacian distributed weights, we know that $k \approx 0.37n$. Thus, the above inequality can be rewritten as

$$\tilde{w}_{k+1} < \mathcal{L}_{\mathbf{b}_w}^k (\sqrt{0.37n+1} - \sqrt{0.37n}). \quad (23)$$

Since n is typically thousands for a neural network and we statistically find that $\mathcal{L}_{\mathbf{b}_w}^k$ ranges from 0.63 to 0.73, the multiplication of the two terms in Eq. (23) thus results in an extremely small \tilde{w}_{k+1} approximating to zero. Thus, we need to enlarge the value of \tilde{w}_{k+1} to break the above inequality. We realize that one of the major causes for a small \tilde{w}_{k+1} lies in the existence of the ℓ_2 regularization imposed on the training of neural network. This inspires us to remove the ℓ_2 regularization for the to-be-binarized weights \mathbf{w} .

As shown in Fig. 2(b), the removal of the ℓ_2 regularization increases the proportion of +1s in $\bar{\mathbf{b}}_w$ to around 51%. We then further enforce the ideal half-half binarization $\tilde{\mathbf{b}}_w$ using Eq. (20). As a result, $k \approx 0.51n$ and $r \approx 0.01n$, yielding the much smaller angle bounds of $[\arccos \sqrt{\frac{0.51}{0.51+0.01}}, \arccos \sqrt{\frac{0.51-0.01}{0.51}}] \approx [7.97^\circ, 8.05^\circ]$ between $\tilde{\mathbf{b}}_w$ and $\bar{\mathbf{b}}_w$. This effectively increases the bit entropy and leads to a nearly optimal solution for the learning objective of Eq. (12). Besides, the half-half binarization further reduces the computational complexity of $\mathcal{O}(n \log n)$ to $\mathcal{O}(n)$ since we only need to find the median of $|\mathbf{w}|$, and encode weights into +1s when their magnitude is larger than the median, and 0s otherwise.

The forward and backward processes of SiMaN are summarized in Algorithm 1. During training, we remove the ℓ_2 regularization and adopt the binarization $\mathbf{b}_w \in \{-1, +1\}^n$ transformed from the half-half binarization $\tilde{\mathbf{b}}_w \in \{0, +1\}^n$ for the convolution in Eq. (2). After training, we obtain a network consisting of a binarized weight $\tilde{\mathbf{b}}_w$ for practical deployment on hardware where the convolution is executed using the XNOR and bitcount operations in Eq. (9).

Algorithm 1 Sign-to-Magnitude Network Binarization

Input: An L -layer full-precision network with weights $\mathbf{W}^i = \{\mathbf{w}_1^i, \mathbf{w}_2^i, \dots, \mathbf{w}_{c_{out}^i}^i\}$ ($i = 1, 2, \dots, L$), input images (activations) $\mathbf{A}^1 = \{\mathbf{a}_1^1, \mathbf{a}_2^1, \dots, \mathbf{a}_{c_{in}^1}^1\}$.

1) Forward Propagation:

Remove the ℓ_2 regularization term.

for $i = 1$ **to** L **do**

 Binarize the inputs $(\mathbf{B}_A)^i = \text{sign}(\mathbf{A}^i)$ (Eq. (3));

for $j = 1$ **to** c_{out}^i **do**

 Obtain the half-half binarization $(\tilde{\mathbf{b}}_w)_j^i$ (Eq. (20));

 Obtain the binarization $(\mathbf{b}_w)_j^i = 2 \cdot (\tilde{\mathbf{b}}_w)_j^i - 1$ (the inverse of Eq. (8));

 Conduct the convolution $\mathbf{a}_j^{i+1} \approx \beta_j^i \cdot (\mathbf{b}_w)_j^i \otimes (\mathbf{B}_A)^i$ (Eq. (2));

end for

$\mathbf{A}^{i+1} = \{\mathbf{a}_1^{i+1}, \mathbf{a}_2^{i+1}, \dots, \mathbf{a}_{c_{out}^{i+1}}^{i+1}\};$

end for

2) Backward Propagation:

for $i = L$ **to** 1 **do**

 Compute gradient $\frac{\partial \mathcal{L}}{\partial \mathbf{A}^i} \approx \frac{\partial \mathcal{L}}{\partial (\mathbf{B}_A)^i} \cdot \frac{\partial F(\mathbf{A}^i)}{\partial \mathbf{A}^i}$ (Eq. (4));

for $j = 1$ **to** c_{out}^i **do**

 Compute gradient $\frac{\partial \mathcal{L}}{\partial \mathbf{w}_j^i} \approx \frac{\partial \mathcal{L}}{\partial (\mathbf{b}_w)_j^i}$ (Eq. (6));

end for

end for

3) Weight Updating:

for $i = L$ **to** 1 **do**

for $j = 1$ **to** c_{out}^i **do**

 Update $\mathbf{w}_j^i = \mathbf{w}_j^i - \eta \frac{\partial \mathcal{L}}{\partial \mathbf{w}_j^i}$; # η denotes learning rate

end for

end for

Output: An L -layer binarized network with weights $(\tilde{\mathbf{b}}_w)^i = \{(\tilde{\mathbf{b}}_w)_1^i, (\tilde{\mathbf{b}}_w)_2^i, \dots, (\tilde{\mathbf{b}}_w)_{c_{out}^i}^i\} (i = 1, 2, \dots, L)$.

5. Experiments

To demonstrate the efficacy of the proposed SiMaN binarization scheme, we compare its performance with several state-of-the-art BNNs on two image classification datasets, including CIFAR-10 (Krizhevsky et al., 2009) and ImageNet (Deng et al., 2009).

5.1. Datasets and Experimental Settings

CIFAR-10 (Krizhevsky et al., 2009) consists of 60,000 32×32 images from 10 classes. Each class has 6,000 images. We split the dataset into 50,000 training images and 10,000 testing images. Data augmentation includes random cropping and random flipping, as done in (He et al., 2016) for the training images.

ImageNet (Deng et al., 2009) contains over 1.2 million images for training and 50,000 validation images from 1,000

classes for classification. Following the recent advances in (Qin et al., 2020b; Han et al., 2020; Lin et al., 2020b), the data augmentation includes random cropping and flipping.

Network Structures For CIFAR-10, we binarize ResNet-18/20 (He et al., 2016) and VGG-small (Zhang et al., 2018). For ImageNet, ResNet-18/34 are chosen for binarization. Following (Qin et al., 2020b; Han et al., 2020; Lin et al., 2020b), double skip connections (Liu et al., 2018) are added to the ResNets and we do not binarize the first and last layers for all networks.

Implementation Details We implement our SiMaN using Pytorch (Paszke et al., 2019) and all experiments are conducted on NVIDIA Tesla V100 GPUs. We use the cosine scheduler with a learning rate of 0.1 (Qin et al., 2020b; Lin et al., 2020b). The SGD is adopted as the optimizer with a momentum of 0.9. For those layers that are not binarized, the weight decay is set to 5×10^{-4} on CIFAR-10 and 1×10^{-4} on ImageNet, and 0 otherwise to remove the ℓ_2 regularization for the bit entropy maximization as discussed in Sec. 4.3. We train the models from scratch with 400 epochs and a batch size of 256 on CIFAR-10, and with 150 epochs and a batch size of 512 on ImageNet.

Note that, we only apply the classification loss during network training for fair comparison. Other training losses such as those proposed in (Hou et al., 2016; Ding et al., 2019; Wang et al., 2019), the variants of network structures in (Bethge et al., 2020; Zhu et al., 2019; Liu et al., 2020), and even the two-step training strategy (Martinez et al., 2019) can be integrated to further boost the binarized networks’ performance. These, however, are not considered here. We aim to show the advantages of our magnitude-based optimization solution over the traditional sign-based methods under regular training loss, the same network structure and a common training strategy.

5.2. Convergence

We first show the convergence ability of our SiMaN, and compare it with another angle alignment-based RBNN, which implements network binarization with the sign function (Lin et al., 2020b). The experiments in Fig. 3 show that our sign-to-magnitude weight binarization has a significantly better ability to converge during BNN training than the traditional sign-based optimization on both training and validation sets, which demonstrates the feasibility of our discrete solution in learning BNNs.

5.3. Ablation Studies

Our SiMaN is built by removing the ℓ_2 regularization and enforcing the half-half strategy in Eq. (20). To analyze their influence, in Table 1, we develop three variants, including (1) SiMaN₁: The ℓ_2 regularization is added while removing

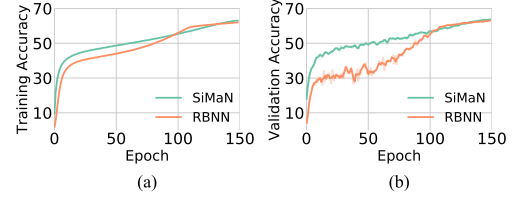


Figure 3. Comparison of training and validation accuracy curves between our SiMaN and RBNN (ResNet-34 on ImageNet).

Table 1. Ablation studies with/without the ℓ_2 regularization and half-half binarization (ResNet-18 on ImageNet).

	ℓ_2 regularization	half-half	Top-1(%)	Top-5(%)
SiMaN ₁	✓	✗	55.1	75.5
SiMaN ₂	✗	✗	57.3	77.4
SiMaN ₃	✓	✓	59.2	81.5
SiMaN	✗	✓	60.1	82.3

the half-half binarization. This variant simply implements binarization based on the proof process of Corollary 1. It results in around 37% of weights encoded into +1s, as analyzed in Corollary 2, which fails to maximize the entropy information, and thus leads to poorer accuracies of 55.1% for the top-1 and 75.5% for the top-5. (2) SiMaN₂: Both the ℓ_2 regularization and the half-half binarization are removed. It shows better top-1 (57.3%) and top-5 (77.4%) accuracies since the removal of the ℓ_2 regularization breaks the Laplacian distribution and results in around 51% of weights being encoded into +1s as experimentally verified in Fig. 2. (3) SiMaN₃: Both the ℓ_2 regularization and the half-half binarization are added. Though the performance increases, it is still limited. This is because, the half-half binarization with the ℓ_2 regularization causes a large angle deviation of around $30.66^\circ - 36.35^\circ$ as analyzed in Sec. 4.3, from the optimal binarization of our learning objective in Eq. (12).

Based on SiMaN₃, our SiMaN further removes the ℓ_2 regularization. On one hand, this ensures the maximal bit entropy; on the other hand, it ensures that the half-half binarization closely matches the optimal binarization (only $7.97^\circ - 8.05^\circ$ angle deviation as analyzed in Sec. 4.3), thereby leading to the best performance in Table 1.

5.4. Results on CIFAR-10

We first conduct detailed studies on CIFAR-10 for the proposed SiMaN as shown in Table 2. As can be seen, our sign-to-magnitude binarization consistently outperforms the recent sign-based state-of-the-arts. Specifically, SiMaN outperforms RBNN (Lin et al., 2020b), IR-Net (Qin et al., 2020b) and SLB (Yang et al., 2020) by 0.3%, 0.9% and 0.5% in binarizing ResNet-18, ResNet-20 and VGG-small, respectively. The results emphasize the importance of building discrete optimization to pursue high-quality weight binarization. Importantly, compared with another angle

Table 2. Comparison with the state-of-the-arts on CIFAR-10. W/A denotes the bit length of the weights and activations. Top-1 accuracy is reported.

Network	Method	W/A	Top-1 (%)
ResNet-18	Full-precision	32/32	94.8
	RAD (Ding et al., 2019)	1/1	90.5
	IR-Net (Qin et al., 2020b)	1/1	91.5
	RBNN (Lin et al., 2020b)	1/1	92.2
	SiMaN (Ours)	1/1	92.5
ResNet-20	Full-precision	32/32	92.1
	DoReFa (Zhou et al., 2016)	1/1	79.3
	DSQ (Gong et al., 2019)	1/1	84.1
	SLB (Yang et al., 2020)	1/1	85.5
	LNS (Han et al., 2020)	1/1	85.8
	IR-Net (Qin et al., 2020b)	1/1	86.5
	SiMaN (Ours)	1/1	87.4
VGG-small	Full-precision	32/32	94.1
	XNOR (Rastegari et al., 2016)	1/1	89.8
	BNN (Courbariaux et al., 2016)	1/1	89.9
	DoReFa (Zhou et al., 2016)	1/1	90.2
	RAD (Ding et al., 2019)	1/1	90.0
	DSQ (Gong et al., 2019)	1/1	91.7
	IR-Net (Qin et al., 2020b)	1/1	90.4
	RBNN (Lin et al., 2020b)	1/1	91.3
	SLB (Yang et al., 2020)	1/1	92.0
	SiMaN (Ours)	1/1	92.5

alignment-based method, *i.e.*, RBNN, our SiMaN increases the performance to 92.5% when binarizing VGG-small, leading to a performance gain of 1.2%. Besides, SiMaN also merits in its easy implementation, where the median of absolute weights acts as the boundary between 0s and +1s to ensure the bit entropy maximization, while the angle alignment is also guaranteed, as analyzed in Sec. 4.3. In contrast, RBNN has to learn two complex rotation matrices and applies them in the beginning phase of each training epoch to reduce the angle bias.

5.5. Results on ImageNet

We also conduct similar experiments on ImageNet to validate the performance of SiMaN on a large-scale dataset. Two common networks, ResNet-18 and ResNet-34, are adopted for binarization. Table 3 shows the results of SiMaN and several other binarization methods. The performance of SiMaN on ImageNet also takes the leading place. Specifically, with ResNet-18, SiMaN achieves 60.1% top-1 and 82.3% top-5 accuracies, respectively, with 0.2% and 0.4% improvements over RBNN. With ResNet-34, it achieves a top-1 accuracy of 63.9% and a top-5 accuracy of 84.8%, outperforming RBNN by 0.8% and 0.4%, respectively.

Table 3. Comparison with the state-of-the-arts on ImageNet. W/A denotes the bit length of the weights and activations. Both top-1 and top-5 accuracies are reported.

Network	Method	W/A	Top-1 (%)	Top-5 (%)
ResNet-18	Full-precision	32/32	69.6	89.2
	BNN (Courbariaux et al., 2016)	1/1	42.2	67.1
	XNOR (Rastegari et al., 2016)	1/1	51.2	73.2
	DoReFa (Zhou et al., 2016)	1/2	53.4	-
	HWGQ (Cai et al., 2017)	1/2	59.6	82.2
	TBN (Wan et al., 2018)	1/2	55.6	79.0
	Bi-Real (Liu et al., 2018)	1/1	56.4	79.5
	PDNN (Gu et al., 2019a)	1/1	57.3	80.0
	BONN (Gu et al., 2019b)	1/1	59.3	81.6
	Si-BNN (Wang et al., 2020)	1/1	59.7	81.8
	IR-Net (Qin et al., 2020b)	1/1	58.1	80.0
	LNS (Han et al., 2020)	1/1	59.4	81.7
	RBNN (Lin et al., 2020b)	1/1	59.9	81.9
	SiMaN (Ours)	1/1	60.1	82.3
ResNet-34	Full-precision	32/32	73.3	91.3
	ABC-Net (Lin et al., 2017)	1/1	52.4	76.5
	Bi-Real (Liu et al., 2018)	1/1	62.2	83.9
	IR-Net (Qin et al., 2020b)	1/1	62.9	84.1
	RBNN (Lin et al., 2020b)	1/1	63.1	84.4
	SiMaN (Ours)	1/1	63.9	84.8

The performance improvements in Table 2 and Table 3 strongly demonstrate the impact of exploring discrete optimization and the effectiveness of our magnitude-based discrete solution in constructing a high-performing BNN.

6. Conclusion

In this paper, we proposed a novel sign-to-magnitude network binarization (SiMaN) scheme that avoids the dependency on the sign function, to optimize a binary neural network for higher accuracy. Our SiMaN reformulates the angle alignment between the weight vector and its binarization as being constrained to $\{0, +1\}$. We proved that an analytical discrete solution can be attained in a computationally efficient manner by encoding into +1s the high-magnitude weights, and 0s otherwise. We also mathematically proved that the learned weights roughly follow a Laplacian distribution, which is harmful to bit entropy maximization. To address the problem, we have shown that simply removing the ℓ_2 regularization during network training can break the Laplacian distribution and lead to a half-half distribution of binarized weights. As a result, the complexity of our binarization could be further simplified by encoding into +1 weights within the largest top-half magnitude, and 0 otherwise. Our experimental results demonstrate the significant performance improvement of SiMaN.

References

- Alizadeh, M., Fernández-Marqués, J., Lane, N. D., and Gal, Y. An empirical study of binary neural networks' optimisation. In *Proceedings of the International Conference on Learning Representations (ICLR)*, 2018.
- Anderson, A. G. and Berg, C. P. The high-dimensional geometry of binary neural networks. In *International Conference on Learning Representations (ICLR)*, 2018.
- Banner, R., Nahshan, Y., Hoffer, E., and Soudry, D. Post-training 4-bit quantization of convolution networks for rapid-deployment. *arXiv preprint arXiv:1810.05723*, 2018.
- Bengio, Y., Léonard, N., and Courville, A. Estimating or propagating gradients through stochastic neurons for conditional computation. *arXiv preprint arXiv:1308.3432*, 2013.
- Bethge, J., Yang, H., Bornstein, M., and Meinel, C. Back to simplicity: How to train accurate bnns from scratch? *arXiv preprint arXiv:1906.08637*, 2019.
- Bethge, J., Bartz, C., Yang, H., Chen, Y., and Meinel, C. Meliusnet: Can binary neural networks achieve mobilenet-level accuracy? *arXiv preprint arXiv:2001.05936*, 2020.
- Bulat, A. and Tzimiropoulos, G. Xnor-net++: Improved binary neural networks. In *Proceedings of the British Machine Vision Conference (BMVC)*, 2019.
- Cai, Z., He, X., Sun, J., and Vasconcelos, N. Deep learning with low precision by half-wave gaussian quantization. In *Proceedings of the IEEE Conference on Computer Vision and Pattern Recognition (CVPR)*, pp. 5918–5926, 2017.
- Conforti, M., Cornuéjols, G., Zambelli, G., et al. *Integer programming*, volume 271. 2014.
- Courbariaux, M., Hubara, I., Soudry, D., El-Yaniv, R., and Bengio, Y. Binarized neural networks: Training deep neural networks with weights and activations constrained to+ 1 or-1. *arXiv preprint arXiv:1602.02830*, 2016.
- Darabi, S., Belbahri, M., Courbariaux, M., and Nia, V. P. Bnn+: Improved binary network training. *arXiv preprint arXiv:1812.11800*, 2018.
- Deng, J., Dong, W., Socher, R., Li, L.-J., Li, K., and Fei-Fei, L. Imagenet: A large-scale hierarchical image database. In *Proceedings of the IEEE Conference on Computer Vision and Pattern Recognition (CVPR)*, pp. 248–255, 2009.
- Ding, R., Chin, T.-W., Liu, Z., and Marculescu, D. Regularizing activation distribution for training binarized deep networks. In *Proceedings of the IEEE Conference on Computer Vision and Pattern Recognition (CVPR)*, pp. 11408–11417, 2019.
- Evci, U., Gale, T., Menick, J., Castro, P. S., and Elsen, E. Rigging the lottery: Making all tickets winners. In *Proceedings of the International Conference on Machine Learning (ICML)*, pp. 2943–2952, 2020.
- Gong, R., Liu, X., Jiang, S., Li, T., Hu, P., Lin, J., Yu, F., and Yan, J. Differentiable soft quantization: Bridging full-precision and low-bit neural networks. In *Proceedings of the IEEE International Conference on Computer Vision (ICCV)*, pp. 4852–4861, 2019.
- Gu, J., Li, C., Zhang, B., Han, J., Cao, X., Liu, J., and Doermann, D. Projection convolutional neural networks for 1-bit cnns via discrete back propagation. In *Proceedings of the AAAI Conference on Artificial Intelligence (AAAI)*, pp. 8344–8351, 2019a.
- Gu, J., Zhao, J., Jiang, X., Zhang, B., Liu, J., Guo, G., and Ji, R. Bayesian optimized 1-bit cnns. In *Proceedings of the IEEE International Conference on Computer Vision (ICCV)*, pp. 4909–4917, 2019b.
- Han, K., Wang, Y., Xu, Y., Xu, C., Wu, E., and Xu, C. Training binary neural networks through learning with noisy supervision. In *Proceedings of the International Conference on Machine Learning (ICML)*, pp. 4017–4026, 2020.
- Hayashi, K., Yamaguchi, T., Sugawara, Y., and Maeda, S.-i. Exploring unexplored tensor network decompositions for convolutional neural networks. In *Proceedings of the Advances in Neural Information Processing Systems (NeurIPS)*, pp. 5552–5562, 2019.
- He, K., Zhang, X., Ren, S., and Sun, J. Deep residual learning for image recognition. In *Proceedings of the IEEE Conference on Computer Vision and Pattern Recognition (CVPR)*, pp. 770–778, 2016.
- Helwegen, K., Widdicombe, J., Geiger, L., Liu, Z., Cheng, K.-T., and Nusselder, R. Latent weights do not exist: Rethinking binarized neural network optimization. In *Proceedings of the Advances in Neural Information Processing Systems (NeurIPS)*, pp. 7533–7544, 2019.
- Hou, L., Yao, Q., and Kwok, J. T. Loss-aware binarization of deep networks. In *Proceedings of the International Conference on Learning Representations (ICLR)*, 2016.
- Howard, A. G., Zhu, M., Chen, B., Kalenichenko, D., Wang, W., Weyand, T., Andreetto, M., and Adam, H. Mobilenets: Efficient convolutional neural networks for mobile vision applications. *arXiv preprint arXiv:1704.04861*, 2017.

- Hubara, I., Courbariaux, M., Soudry, D., El-Yaniv, R., and Bengio, Y. Binarized neural networks. In *Proceedings of the Advances in Neural Information Processing Systems (NeurIPS)*, pp. 4107–4115, 2016.
- Jaderberg, M., Vedaldi, A., and Zisserman, A. Speeding up convolutional neural networks with low rank expansions. In *Proceedings of the British Machine Vision Conference (BMVC)*, 2014.
- Kim, H., Khan, M. U. K., and Kyung, C.-M. Efficient neural network compression. In *Proceedings of the IEEE Conference on Computer Vision and Pattern Recognition (CVPR)*, pp. 12569–12577, 2019.
- Krizhevsky, A., Hinton, G., et al. Learning multiple layers of features from tiny images. 2009.
- Leng, C., Dou, Z., Li, H., Zhu, S., and Jin, R. Extremely low bit neural network: Squeeze the last bit out with admm. In *Proceedings of the AAAI Conference on Artificial Intelligence (AAAI)*, 2018.
- Lin, M., Ji, R., Wang, Y., Zhang, Y., Zhang, B., Tian, Y., and Shao, L. Hrank: Filter pruning using high-rank feature map. In *Proceedings of the IEEE Conference on Computer Vision and Pattern Recognition (CVPR)*, pp. 1529–1538, 2020a.
- Lin, M., Ji, R., Xu, Z., Zhang, B., Wang, Y., Wu, Y., Huang, F., and Lin, C.-W. Rotated binary neural network. In *Proceedings of the Advances in Neural Information Processing Systems (NeurIPS)*, 2020b.
- Lin, M., Ji, R., Zhang, Y., Zhang, B., Wu, Y., and Tian, Y. Channel pruning via automatic structure search. In *Proceedings of the International Joint Conference on Artificial Intelligence (IJCAI)*, pp. 673–679, 2020c.
- Lin, X., Zhao, C., and Pan, W. Towards accurate binary convolutional neural network. In *Proceedings of the Advances in Neural Information Processing Systems (NeurIPS)*, pp. 345–353, 2017.
- Liu, Z., Wu, B., Luo, W., Yang, X., Liu, W., and Cheng, K.-T. Bi-real net: Enhancing the performance of 1-bit cnns with improved representational capability and advanced training algorithm. In *Proceedings of the European Conference on Computer Vision (ECCV)*, pp. 722–737, 2018.
- Liu, Z., Shen, Z., Savvides, M., and Cheng, K.-T. Reactnet: Towards precise binary neural network with generalized activation functions. In *Proceedings of the European Conference on Computer Vision (ECCV)*, pp. 143–159, 2020.
- Long, J., Shelhamer, E., and Darrell, T. Fully convolutional networks for semantic segmentation. In *Proceedings of the IEEE Conference on Computer Vision and Pattern Recognition (CVPR)*, pp. 3431–3440, 2015.
- Martinez, B., Yang, J., Bulat, A., and Tzimiropoulos, G. Training binary neural networks with real-to-binary convolutions. In *International Conference on Learning Representations (ICLR)*, 2019.
- Paszke, A., Gross, S., Massa, F., Lerer, A., Bradbury, J., Chanan, G., Killeen, T., Lin, Z., Gimelshein, N., Antiga, L., et al. Pytorch: An imperative style, high-performance deep learning library. In *Proceedings of the Advances in Neural Information Processing Systems (NeurIPS)*, pp. 8026–8037, 2019.
- Peters, J. W. and Welling, M. Probabilistic binary neural networks. *arXiv preprint arXiv:1809.03368*, 2018.
- Qin, H., Gong, R., Liu, X., Bai, X., Song, J., and Sebe, N. Binary neural networks: A survey. *Pattern Recognition (PR)*, 105:107281, 2020a.
- Qin, H., Gong, R., Liu, X., Shen, M., Wei, Z., Yu, F., and Song, J. Forward and backward information retention for accurate binary neural networks. In *Proceedings of the IEEE Conference on Computer Vision and Pattern Recognition (CVPR)*, pp. 2250–2259, 2020b.
- Rastegari, M., Ordonez, V., Redmon, J., and Farhadi, A. Xnor-net: Imagenet classification using binary convolutional neural networks. In *Proceedings of the European Conference on Computer Vision (ECCV)*, pp. 525–542, 2016.
- Redmon, J., Divvala, S., Girshick, R., and Farhadi, A. You only look once: Unified, real-time object detection. In *Proceedings of the IEEE Conference on Computer Vision and Pattern Recognition (CVPR)*, pp. 779–788, 2016.
- Shakarji, C. M. and Srinivasan, V. Theory and algorithms for weighted total least-squares fitting of lines, planes, and parallel planes to support tolerancing standards. *Journal of Computing and Information Science in Engineering*, 13(3), 2013.
- Shayer, O., Levi, D., and Fetaya, E. Learning discrete weights using the local reparameterization trick. In *Proceedings of the International Conference on Learning Representations (ICLR)*, 2018.
- Simons, T. and Lee, D.-J. A review of binarized neural networks. *Electronics*, 8(6):661, 2019.
- Wan, D., Shen, F., Liu, L., Zhu, F., Qin, J., Shao, L., and Tao Shen, H. Tbn: Convolutional neural network with ternary inputs and binary weights. In *Proceedings of the European Conference on Computer Vision (ECCV)*, pp. 315–332, 2018.

Wang, P., He, X., Li, G., Zhao, T., and Cheng, J. Sparsity-inducing binarized neural networks. In *Proceedings of the AAAI Conference on Artificial Intelligence (AAAI)*, pp. 12192–12199, 2020.

Wang, Z., Lu, J., Tao, C., Zhou, J., and Tian, Q. Learning channel-wise interactions for binary convolutional neural networks. In *Proceedings of the IEEE Conference on Computer Vision and Pattern Recognition (CVPR)*, pp. 568–577, 2019.

Yang, J., Shen, X., Xing, J., Tian, X., Li, H., Deng, B., Huang, J., and Hua, X.-s. Quantization networks. In *Proceedings of the IEEE Conference on Computer Vision and Pattern Recognition (CVPR)*, pp. 7308–7316, 2019.

Yang, Z., Wang, Y., Han, K., Xu, C., Xu, C., Tao, D., and Xu, C. Searching for low-bit weights in quantized neural networks. In *Proceedings of the Advances in Neural Information Processing Systems (NeurIPS)*, 2020.

Zhang, D., Yang, J., Ye, D., and Hua, G. Lq-nets: Learned quantization for highly accurate and compact deep neural networks. In *Proceedings of the European Conference on Computer Vision (ECCV)*, pp. 365–382, 2018.

Zhong, K., Zhao, T., Ning, X., Zeng, S., Guo, K., Wang, Y., and Yang, H. Towards lower bit multiplication for convolutional neural network training. *arXiv preprint arXiv:2006.02804*, 2020.

Zhou, S., Wu, Y., Ni, Z., Zhou, X., Wen, H., and Zou, Y. Dorefa-net: Training low bitwidth convolutional neural networks with low bitwidth gradients. *arXiv preprint arXiv:1606.06160*, 2016.

Zhu, S., Dong, X., and Su, H. Binary ensemble neural network: More bits per network or more networks per bit? In *Proceedings of the IEEE Conference on Computer Vision and Pattern Recognition (CVPR)*, pp. 4923–4932, 2019.

A. The practical proportion of +1s.

We further display more about the practical proportion of weights being encoded into +1s in different layers of different networks when trained with and without the ℓ_2 regularization to support our Corollary 2 that $w \in \mathbf{w}$ roughly follows a zero-mean Laplacian distribution.

From Figs. 4–12, we can see that, the proportion of +1s trained with ℓ_2 regularization, falls into the range between 0.36 and 0.38, which is very close to the theoretical result of 0.37 for the Laplacian distribution. Thus, the trained weights follow the Laplacian distribution. By removing the ℓ_2 regularization during network training, the proportion of

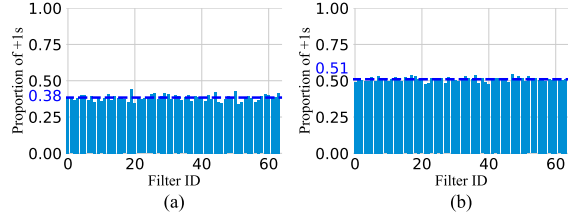


Figure 4. Proportion of +1s trained (a) with and (b) without the ℓ_2 regularization (Layer1.1.2 of ResNet-18). The dashed blue lines denote the average proportions of +1s of all filter weights (Best view with zooming in).

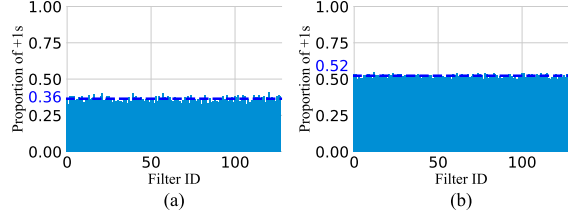


Figure 5. Proportion of +1s trained (a) with and (b) without the ℓ_2 regularization (Layer2.1.2 of ResNet-18). The dashed blue lines denote the average proportions of +1s of all filter weights (Best view with zooming in).

+1s increases to the range between 0.50 and 0.52, which is very close to the ideal half-half distribution.

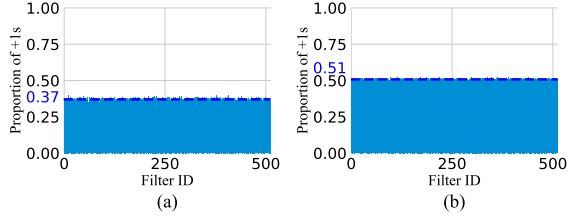


Figure 6. Proportion of +1s trained (a) with and (b) without the ℓ_2 regularization (Layer4.1.2 of ResNet-18). The dashed blue lines denote the average proportions of +1s of all filter weights (Best view with zooming in).

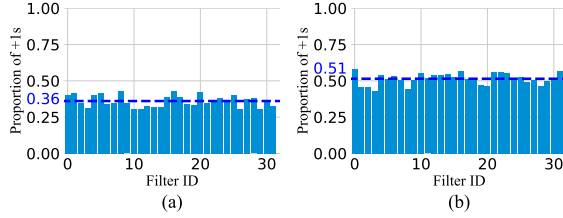


Figure 7. Proportion of +1s trained (a) with and (b) without the ℓ_2 regularization (Layer2.1.2 of ResNet-20). The dashed blue lines denote the average proportions of +1s of all filter weights (Best view with zooming in).

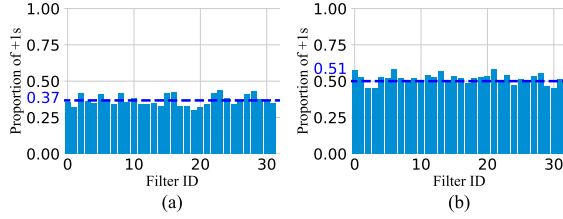


Figure 8. Proportion of +1s trained (a) with and (b) without the ℓ_2 regularization (Layer2.2.2 of ResNet-20). The dashed blue lines denote the average proportions of +1s of all filter weights (Best view with zooming in).

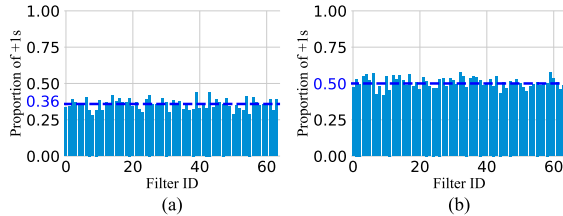


Figure 9. Proportion of +1s trained (a) with and (b) without the ℓ_2 regularization (Layer3.2.1 of ResNet-20). The dashed blue lines denote the average proportions of +1s of all filter weights (Best view with zooming in).

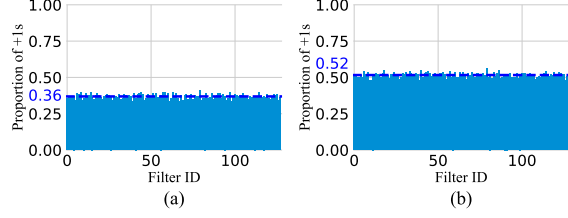


Figure 10. Proportion of +1s trained (a) with and (b) without the ℓ_2 regularization (Layer1 of VGG). The dashed blue lines denote the average proportions of +1s of all filter weights (Best view with zooming in).

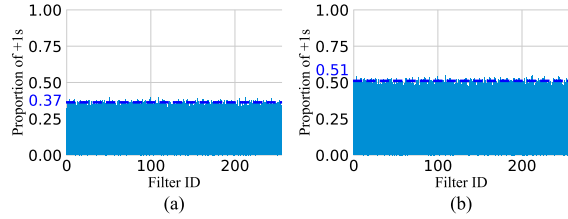


Figure 11. Proportion of +1s trained (a) with and (b) without the ℓ_2 regularization (Layer2 of VGG). The dashed blue lines denote the average proportions of +1s of all filter weights (Best view with zooming in).

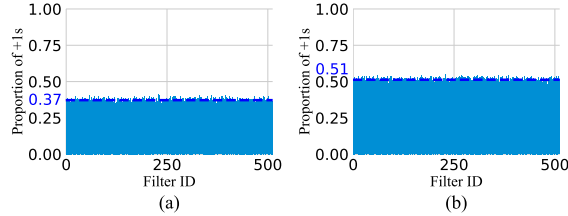


Figure 12. Proportion of +1s trained (a) with and (b) without the ℓ_2 regularization (Layer4 of VGG). The dashed blue lines denote the average proportions of +1s of all filter weights (Best view with zooming in).